The highly resolved electronic spectrum of the square planar $CuCl_4^{2-}$ ion

Andrew Dick,[1] Hedayat Rahemi,[2] Elmars R. Krausz,[3] Graeme R. Hanson,[4] and Mark J. Riley[1,a)]
[1]*School of Molecular and Microbial Sciences, University of Queensland, St. Lucia, Queensland 4072, Australia*
[2]*Chemistry Department, Urmia University, Urmia 57159-165, Iran*
[3]*Research School of Chemistry, Australian National University, Canberra 0200, Australia*
[4]*Centre for Magnetic Resonance, University of Queensland, St. Lucia, Queensland 4072, Australia*

(Received 9 October 2008; accepted 31 October 2008; published online 5 December 2008)

The low temperature magnetic circular dichroism (MCD) and electron paramagnetic resonance (EPR) spectra of Cu(II) doped Cs_2ZrCl_6 are reported. The Cu(II) ion is incorporated as the square planar copper tetrachloride ion, $CuCl_4^{2-}$, which substitutes at the Zr(IV) site in the Cs_2ZrCl_6 lattice, with a complete absence of axial coordination. Both the EPR and MCD show highly resolved spectra from which it is possible to determine the superhyperfine coupling constants and excited state geometries respectively. The Franck–Condon intensity patterns suggest that there is a substantial relaxation of the host lattice about the impurity ion. For the lowest energy $^2B_{1g}(x^2\text{-}y^2) \rightarrow {}^2B_{2g}(xy)$ transition, both the magnetic dipole allowed electronic origin as well as vibronic false origins are observed. The high resolution of the spectra allowed the accurate determination of the odd parity vibrations that are active in the spectra. The opposite sign of the MCD of the two components of the $^2E_g(xz,yz)$ excited state allows this splitting to be determined for the first time. Accurate and unambiguous spectral parameters for the $CuCl_4^{2-}$ ion are important as it has become a benchmark transition metal complex for theoretical electronic structure calculations.
 [DOI: 10.1063/1.3033367]

I. INTRODUCTION

The Jahn–Teller effect precludes the $CuCl_4^{2-}$ anion from adopting a tetrahedral geometry, where it is predominately found in the solid state as a compressed tetrahedron with D_{2d} symmetry. However, it is also possible for the $CuCl_4^{2-}$ ion to occur with the centrosymmetric, square planar D_{4h} geometry.[1] In all reported cases,[2] the compounds that contain the planar $CuCl_4^{2-}$ ion, also have one or more large organic counter ions that stabilize the square planar geometry by forming a hydrogen-bonding network. Recently, we have found that $CuCl_4^{2-}$ can be doped into the Cs_2ZrCl_6 lattice and adopts a square planar geometry in the absence of hydrogen bonding.[3] The only other example of a square planar $CuCl_4^{2-}$ ion occurring in a doped system is in the host K_2PdCl_4, where the geometry was confirmed by electron paramagnetic resonance (EPR) spectroscopy.[4]

Strict square planar $CuCl_4^{2-}$ ions with no axial coordination have a very characteristic electronic absorption spectrum.[5] As the geometry of the $CuCl_4^{2-}$ ion changes from a D_{2d} distorted tetrahedron to the D_{4h} square planar geometry, the *d-d* absorption bands shift to higher energy.[1] In particular, the energy of the $^2B_{1g}(x^2\text{-}y^2) \rightarrow {}^2A_{1g}(z^2)$ transition is substantially increased due to the depression of the energy of the d_{z^2} orbital caused by $3d\text{-}4s$ mixing as both the d_{z^2} and $4s$ orbitals have a_{1g} symmetry in the D_{4h} point group.[6]

As well as being shifted to higher energy, the *d-d* absorption bands of the square planar complex are of interest as they can show extensive vibrational fine structure at low temperature. This is because all transitions to excited states involve the promotion of an electron to the $d_{x^2-y^2}$ orbital which points directly at the four Cl^- ligands. This leads to an expansion of all four bonds in the excited state. The excited state potential energy surfaces as a function of the totally symmetric stretching vibrational coordinate will have their minimum displaced with respect to that of the ground state potential surface. This leads to long Franck–Condon progressions in the totally symmetric mode, and this vibrational structure can be analyzed to determine the bond length change in the excited electronic states.

Accurate and unambiguous spectral parameters for the $CuCl_4^{2-}$ ion are important as it has become a benchmark transition metal complex for theoretical electronic structure calculations, and also has been used as a calibrant to adjust functionals to fit the spectroscopic properties.[7] In particular, the highly resolved magnetic circular dichroism (MCD) spectra presented here offer some new insights to the electronic structure of this complex.

II. EXPERIMENTAL SECTION

Samples of 1% copper(II) doped into a Cs_2ZrCl_6 host crystal were prepared as described previously.[3] The crystals were hygroscopic and all measurements were made on freshly cleaved samples. The Cs_2ZrCl_6 host belongs to the cubic space group $Fm3m$, which has an antifluorite type structure ($\mathbf{a}=1040.7\pm0.5$ pm, $Z=4$).[8] This lattice contains isolated $ZrCl_6^{2-}$ octahedra with a Zr–Cl bond length of 245 ± 2 pm. These octahedra can accommodate different

a)Author to whom correspondence should be addressed. Electronic mail: m.riley@uq.edu.au.

sized guest ions without destroying the O_h symmetry of the Zr(IV) site. The host lattice is reported to both cleave along the (111) planes,[9] and along cubic directions.[10] Here we have used the (001) face for MCD measurements.

A. Experimental MCD spectroscopy

Total and differential circularly polarized light intensity were measured simultaneously using a single beam instrument consisting of a 250 W tungsten lamp dispersed by a Jobin/Yvon 750 S monochromator.[11] The beam was linearly polarized by a calcite crystal (extinction $<10^{-6}$), mechanically chopped at 500 Hz (New Focus 3501), circularly polarized by a photoelastic modulator at a frequency of 42 kHz (Hinds PEM II/IS42), and passed through the sample held in an Oxford Instruments Spectromag 7 T superconducting magnet. Light was detected either with a S-5 photomultiplier (Hamamatsu R7459; 300–700 nm) or InGaAs photodiode detector (UDT sensors 3 mm; 700–1700 nm) and the signal extracted with two lock-in amplifiers (Stanford SR830). All instrument control and data collection was achieved with GPIB protocols and LABVIEW software.

B. Electron paramagnetic resonance

Single crystal *Q*-band EPR spectra were measured on a Bruker ESP300E spectrometer. Temperature control of the sample was achieved by using a helium flow cryostat (Oxford Instruments CF935) in conjunction with an Oxford Instruments ITC4 temperature controller and all spectra were recorded at 16 K. The microwave frequency and magnetic field were calibrated by an EIP845B microwave frequency counter and a Bruker ER035M gauss meter. Simulations of the EPR spectra were performed with version 1.1.4 of the XSOPHE-SOPHE-XEPRVIEW software suite using matrix diagonalization while treating the Cl superhyperfine interactions with perturbation theory.[12]

III. RESULTS AND DISCUSSION

The Cs_2ZrCl_6 lattice is a popular host material for optical studies on M^{4+} hexahalide ions such as $PaCl_6^{2-}$,[13] and $PtCl_6^{2-}$,[14] due to its transparency extending to 320 nm and high symmetry. The host lattice is also well suited for luminescence studies as it lacks high energy vibrations which cause radiationless relaxation. It is also known that Pt^{2+} and Pd^{2+} ions can be doped into the Cs_2ZrCl_6 lattice,[15] where the $PtCl_4^{2-}$ and $PdCl_4^{2-}$ ions replace a $ZrCl_6^{2-}$ ion so that there are chloride vacancies in the axial positions without requiring charge compensation. The O_h site of the Zr in the lattice is reduced to the local D_{4h} symmetry when replaced by the Cu(II) and associated vacancies.

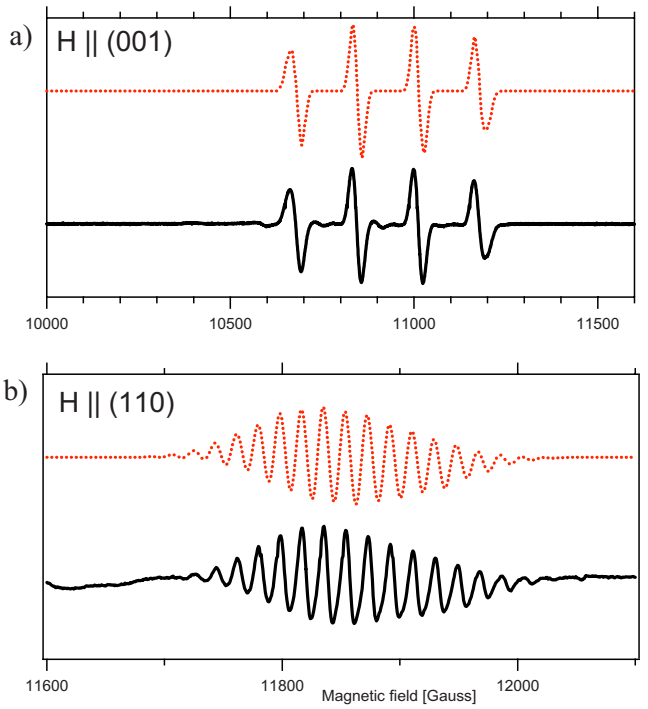

FIG. 1. (Color online) The *Q*-band EPR spectrum of $Cu(II)/Cs_2ZrCl_6$ (a) $H\|(001)$ and (b) $H\|(110)$ at 16 K using a microwave frequency of 33.9653 GHz. The experimental spectra are given as solid lines, while the spectra simulated using the parameters in Table I are shown as dashed lines.

This is an ideal situation to study this planar ion, as it is known that even distant axial atoms can perturb the energy of the spectra.[5] The tetragonal fourfold axis of the $CuCl_4^{2-}$ ion will substitute into the cubic host lattice so that it is aligned along the *x*, *y*, or *z* cubic axes in a statistical manner. The MCD measurements using the well developed (001) faces will therefore be of two magnetically inequivalent species that are either parallel or perpendicular to the applied field directions.

A. Electron paramagnetic resonance spectra

The single crystal EPR spectra are shown in Fig. 1 and have been fitted to $S=1/2$, $I=3/2$ spin Hamiltonian with the axially symmetric parameters $g_\|$, $g_\perp$, $A_\|$, and $A_\perp$, as given in Table I. In addition, the superhyperfine coupling with the $I=3/2$ nuclear spin on the Cl ligands are described by $A_\|^L$ and $A_\perp^L$ parameters that are axially symmetric with respect to the Cu–Cl bond directions. The principal axis of the hyperfine

TABLE I. Spin Hamiltonian parameters used in the simulation of the EPR spectrum shown in Fig. 1.

Host	$g_\|$	$g_\perp$	$\|A_\|(Cu)\|\times10^{-4}$ cm^{-1}	$\|A_\perp(Cu)\|\times10^{-4}$ cm^{-1}	$\|A_\|(Cl)\|\times10^{-4}$ cm^{-1}	$\|A_\perp(Cl)\|\times10^{-4}$ cm^{-1}
Cs_2ZrCl_6	2.2202	2.0460	170.2	35.94	23.54	5[a]
(Minority center)	2.242	⋯	163	⋯	⋯	⋯
K_2PdCl_4 [b]	2.232	2.049	163.6	34.5	23.3	5.3

[a]Upper limit. $A_\|(Cu)$ and $A_\perp(Cu)$ are parallel are perpendicular to the C_4 axis of the complex, while $A_\|(Cl)$ and $A_\perp(Cl)$ are with respect to the Cu–Cl bond directions. Parameters for only one isotope are fitted (^{63}Cu and ^{35}Cl).
[b]Reference 4.

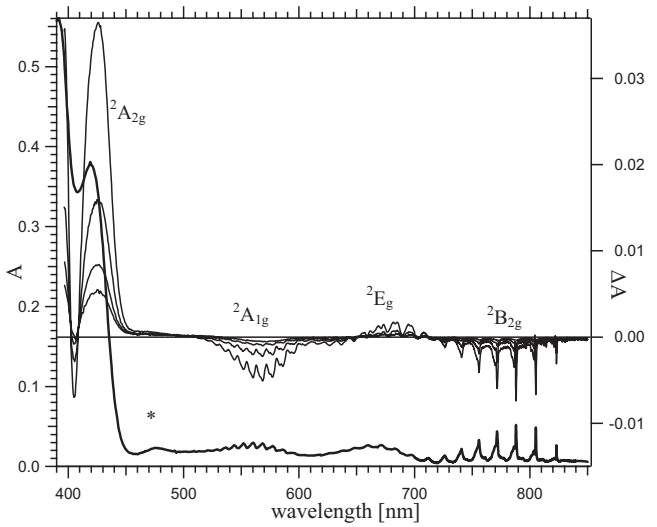

FIG. 2. The low temperature (1.8 K) absorption spectrum (bold, left hand side axis) and the MCD spectra (upper, right hand side axis) of $CuCl_4^{2-}/Cs_2ZrCl_6$. The MCD spectra have been measured at the temperatures 1.8, 10, 25, and 50 K in a field of 7 T. The asterisk denotes an unknown impurity (see text).

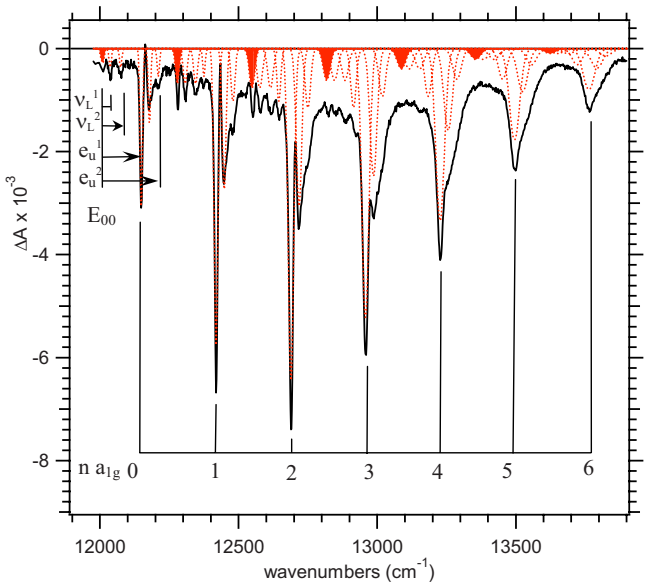

FIG. 3. (Color online) An analysis of the vibrational fine structure in the MCD spectrum of the $^2B_{1g}(x^2\text{-}y^2) \rightarrow {}^2B_{2g}(xy)$ transition. The Franck–Condon progression has been simulated using the parameters given in Table III.

coupling is then 90° to that of $g_\parallel$ and $A_\parallel$. The values obtained are quite similar to those of a previous study[4] of Cu(II) doped K_2PdCl_4 which are also given in Table I for comparison.

The particular orientations of the magnetic field that give rise to the most resolved spectra are the (001) direction [Fig. 1(a)], and the (110) direction [Fig. 1(b)]. In the latter case the magnetic field is at 45° to the Cu–Cl bonds in all centers so that the superhyperfine coupling with the ligands are equivalent, and the four ligands will give rise to thirteen resonances on each of the four ^{63}Cu hyperfine lines. However the ^{63}Cu hyperfine coupling, $A_\perp$, is approximately twice that of the ^{35}Cl superhyperfine coupling in this direction, and this is what gives rise to the resulting 19 resonances in the (110) spectrum, as shown in both the experimental and the simulated spectra in Fig. 1(b). The (001) spectrum in Fig. 1(a) can be used to determine $g_\parallel$ and $A_\parallel$ while the (110) spectrum can be used to fit $g_\perp$, $A_\perp$, and 1/2 $(A_{\parallel L}{}^2+A_{\perp L}{}^2)$. The $A_{\parallel L}$ value must be small as it is not resolved in the (100) spectrum, and we have estimated an upper limit of 5×10^{-4} cm^{-1} for this value. Additional weak features can be seen in the (001) spectrum which we attribute to a minority species which, from the integration of the spectra is <2% of the total Cu(II) ion concentration. These can be fitted to the slightly different axial parameters $g_\parallel=2.242$ and $A_\parallel=163\times10^{-4}$ cm^{-1}.

B. The optical spectrum

The 1.8 K electronic absorption and MCD spectra of ~1% doped $CuCl_4^{2-}/Cs_2ZrCl_6$ are shown in Fig. 2. The absorption spectrum has been previously given at 10 K.[3] The weak structured features in the 500–850 nm spectral region are the well-known ligand field transitions of the square planar $CuCl_4^{2-}$ ion.[5] These ligand field transitions show extensive vibrational fine structure which is particularly resolved in the MCD spectrum, as shown in Fig. 3. The higher energy, more intense transitions <500 nm are also well known as ligand-to-metal charge transfer (LMCT) transitions.[16]

In centrosymmetric symmetry, electric dipole allowed transitions between the ligand field states are parity forbidden. Vibrational sidebands can however by induced by coupling to odd parity vibrations.[17] These sidebands can in turn act as false origins and couple with totally symmetric modes to form a Franck–Condon progression.

The LMCT transitions arise from promoting an electron from the predominantly π bonding orbitals on the Cl ligands, and are much more intense. This is because ungerade states exist which make the transitions electric dipole allowed. The original $X\text{-}\alpha$ (Ref. 18) electronic structure calculations and more recently various flavors of density functional theory,[7] indicate that the states that involve the promotion of an electron from symmetry adapted linear combinations of ligand orbitals with e_u symmetry should dominate in the LMCT spectrum. This result agrees with MCD spectra as the strong MCD intensity in the LMCT region <450 nm in Fig. 2 indicates that the transitions are to excited states with a large amount of orbital angular momentum.

C. Ligand field spectra

In pure compounds containing the planar $CuCl_4^{2-}$ ion, the observed intensity of the ligand field bands is mainly vibronic in nature. Franck–Condon vibrational progressions have been assumed to be built on vibronic origins due to odd parity vibrations.[19] The magnetic dipole allowed electronic origin in the lowest energy transition in crystals of bis(2-aminobenzothiazolium) $CuCl_4$, has been previously observed[20] and the magnetic dipole intensity has been shown to be small compared to the vibronic intensity. In the present case, the observed band maxima of the Franck–Condon envelopes in absorption are at 12 900, 14 750, and

TABLE II. Observed and calculated ligand field transitions.

	No spin-orbit coupling[a]		Nonzero spin-orbit coupling[b]		
Observed (cm^{-1})	Transition	Calculated (cm^{-1})	Transition	Calculation 1 (cm^{-1})	Calculation 2[c] (cm^{-1})
12 900	$^2B_{1g} \rightarrow B_{2g}$	12 900	$\Gamma_7 \rightarrow \Gamma_7$	12 854	12 868
14 750	$\rightarrow {}^2E_g$	14 750	Γ_7	14 616	14 629
			Γ_6	14 897	15 883
17 700	$\rightarrow {}^2A_{1g}$	17 700	Γ_6	17 901	17 886

[a]The observed energies were fitted to the AOM parameters $e_\sigma = 5533\ cm^{-1}$, $e_\pi = 925\ cm^{-1}$, and $e_{ds} = 1658\ cm^{-1}$ (see text).
[b]The $\zeta = 830\ cm^{-1}$, reduced by an orbital reduction factor of $k = 0.68$.
[c]This calculation is with the spin orbit quenched within the ^2E_g excited state.

17 700 cm^{-1} which can be assigned to the vertical transitions of $^2B_{1g}(x^2\text{-}y^2) \rightarrow {}^2B_{2g}(xy)$, $^2E_g(xz,yz)$, $^2A_{1g}(z^2)$ at the ground state geometry respectively, as given in Table II. The energies are similar to those observed for pure copper(II) compounds containing the planar $CuCl_4^{2-}$ ion apart from a small shift to higher energy (see below), confirming this stereochemistry for the dopant in Cu(II) doped Cs_2ZrCl_6.

Using the three band maxima, the angular overlap model (AOM) parameters can be uniquely found as $e_\sigma = 5533\ cm^{-1}$, $e_\pi = 925\ cm^{-1}$, and $e_{ds} = 1658\ cm^{-1}$ using the ligand field program CAMMAG.[21] The observed and calculated energy levels are given in Table II. The AOM parameters are similar to those obtained for other square planar $CuCl_4^{2-}$ systems, but all values are slightly higher. Experimentally this is manifested by the overall shift of the positions of the band maxima to higher energy. This is especially true for the highest energy $^2B_{2g}(x^2\text{-}y^2) \rightarrow {}^2A_{1g}(z^2)$ transition which is some $\sim 1000\ cm^{-1}$ higher in energy than that of other reported square planar $CuCl_4^{2-}$ systems.[5,20] The experimental g-values can be calculated within the lowest Kramers doublet using the above AOM values, and requires an orbital reduction parameter of $k = 0.68$. The values compare well to the covalency obtained for this complex from a variety of experimental and theoretical techniques.[7]

Such a shift may be due to the complete absence of axial ligation, which results in greater $4s\text{-}3d$ mixing and stabilization of the (z^2) d-orbital.[6] The nearest axial atom is a chloride at a distance of 795 pm (and one at 460 pm, 27.9° from the axial direction) due to neighboring $ZrCl_6^{2-}$ centers. The small overall shift to higher energy of all the transitions is unexpected as the host Zr–Cl bond length (245 pm) is substantially greater than the observed Cu–Cl bond length of 226 pm, averaged from the five known planar $CuCl_4^{2-}$ structures.[20] Clearly, with such a bond length difference between guest and host structures, there must be some relaxation of the host lattice around the impurity ion when a $ZrCl_6^{2-}$ center is replaced by $CuCl_4^{2-}$.

Figure 3 shows an expanded view of the $^2B_{1g}(x^2\text{-}y^2) \rightarrow {}^2B_{2g}(xy)$ transition, which exhibits the best resolved vibrational fine structure. The spectra have been fitted to Gaussian peaks that are Franck–Condon progressions based on an electronic (E_{00}) and vibronic origins $\bar{\nu}_i$ using the parameters given in Table III and a sum of Gaussian functions where each Gaussian is characterized by the area (I), width (W),

TABLE III. The parameters used in the simulation of the ligand field MCD spectra in Figs. 3 and 4.

	Transition		
	$^2B_{1g}(x^2\text{-}y^2) \rightarrow {}^2B_{2g}(xy)$	$^2B_{1g}(x^2\text{-}y^2) \rightarrow {}^2E_g(xz,yz)$	$^2B_{1g}(x^2\text{-}y^2) \rightarrow {}^2A_{1g}(z^2)$
E_{00} (cm^{-1})	12 012 (0.075)	14 115.8 (1.00)[a] 14 380.8(−0.69)	16 479 (0)[b]
Vibronic origins[c] (cm^{-1})	$\bar{\nu}_L^1$ +30.5(0.061) $\bar{\nu}_L^2$ +63.6(0.078) $\bar{\nu}_L^3$ +96.4(0.081) $\bar{\nu}e_u^1$ +141(1.00) $\bar{\nu}e_u^2$ +200.1(0.159)		$\bar{\nu}b_{2u}$ +26(1) $\bar{\nu}e_u^1$ +141(0.74)
$\bar{\nu}a_{1g}$ (cm^{-1})	271.5	262.2	271.9
$\bar{\nu}\chi_e a_{1g}$ (cm^{-1})	0.34	−0.17	0.74
W (cm^{-1})	17.05	128.4, 80.6	129.9, 99.9
Δ (cm^{-1})	6.77	6.76, 16.11	0.51, 6.73
D	2.49	2.71	2.98
Δr (pm)	+7.4	+8.2	+8.8

[a]Spin-orbit split components, see text.
[b]The inferred value.
[c]The assignment is given, followed by the wavenumber difference from the origin, and in brackets the area relative to that of the strongest origin.

and position (E) each of which is identified as being the nth member of the Franck–Condon progression on the ith vibronic origin, and are given below:

$$I(i,n) = I_i \frac{D^{2n}}{2^n n!} \exp(-D^2),$$

$$W(i,n) = W_i + \Delta_i n, \tag{1}$$

$$E(i,n) = E_{00} + \bar{\nu}_i + \bar{\nu}a_{1g} - \bar{\nu}\chi_e(n^2+1).$$

The summation is over all possible i vibronic "enabling" modes $\bar{\nu}_i$ and all levels n of the totally symmetric vibration $\bar{\nu}a_{1g}$ in the excited state. (For $n>10$, the area becomes vanishingly small.) The low temperature limit is assumed so that the initial state is the lowest vibrational level in the ground electronic state. In the simulation of the $^2B_{1g}(x^2\text{-}y^2) \rightarrow {}^2B_{2g}(xy)$ transition shown in Fig. 3, the three lowest energy weaker vibronic origins ($\bar{\nu}_L{}^1, \bar{\nu}_L{}^2, \bar{\nu}_L{}^3$) we assign to lattice modes, while the bulk of the intensity of this transition is based on the two vibronic origins $\bar{\nu}e_u{}^1$ and $\bar{\nu}e_u{}^2$.

The $^2B_{1g}(x^2\text{-}y^2) \rightarrow {}^2B_{2g}(xy)$ transition is vibronically allowed only in xy polarization by e_u vibrations. The $CuCl_4^{2-}$ complex has two $\bar{\nu}e_u$ vibrations, which in the ground state, have the energies ~190 and 300 cm^{-1} for the bend and stretch vibrations respectively.[20] With our assignments in the excited state these vibrations appear at the reduced values of ~141 and 200 cm^{-1} (Table III). The majority of the intensity of the $^2B_{1g}(x^2\text{-}y^2) \rightarrow {}^2B_{2g}(xy)$ transition is based on the $\bar{\nu}e_u{}^1$ bending vibration and Fig. 3 shows a clear Franck–Condon progression based on this origin up to $n=6$. The peak/shoulder immediately to higher energy of each of these members we assign to a phonon wing of the main peak rather than to a separate vibronic origin. In a previous study[3] we erroneously assigned the main vibronic origin of the $^2B_{1g}(x^2\text{-}y^2) \rightarrow {}^2B_{2g}(xy)$ transition as a magnetic dipole allowed electric origin, as we were not able not detect the weak features to lower energy in the absorption spectrum. However, these weak origins are readily apparent in the MCD spectrum (Fig. 3).

A major broadening mechanism for the members of a Franck–Condon progression is the 75%/25% natural abundance of the $^{35}Cl/^{37}Cl$ isotopes. The difference in the reduced masses of the five possible combinations of the two isotopes causes the totally symmetric stretching vibration to split into 5 for the first $n=1$ member, 5^2 for $n=2$, etc. The energy difference in the extreme cases $Cu^{35}Cu_4{}^{2-}$ and $Cu^{37}Cu_4{}^{2-}$ is equal to $\bar{\nu}_{35}(n+1)\,[1-\sqrt{35/37}]$, where $\bar{\nu}_{35}$ is the energy of the $Cu^{35}Cu_4{}^{2-}$ vibration.[3,22] This splitting is proportional to n, the member of the progression of the totally symmetric mode. Each member of the progression is therefore expected to broaden as a linear function of n due to this isotope effect. The half widths observed for different members of the Franck–Condon progression based on each vibronic origin do indeed follow this pattern and such broadening is taken into account in the simulation by the parameters Δ_i in Eq. (1) and Table III.

D. Spin-orbit splitting of the $^2E_g(xz,yz)$ state

The spin-orbit splitting of the ^2E_g excited state into the Γ_6, Γ_7 representations of the D_{4h}^* double group is expected to be 281 cm^{-1} using the parameters in Table II, with the Γ_7 state lower. The ^2E_g state is formally subject to a $E_g \otimes (b_{1g}+b_{2g})$ Jahn–Teller effect. This will have the effect of reducing this spin-orbit splitting. The spin-orbit coupling enters as the L_zS_z matrix element in the ^2E_g state, which is an operator of Γ_2 (A_{2g}) symmetry, and such operators are expected to be reduced to zero for a strong Jahn–Teller coupling.[23] To investigate this possibility, we estimated the Jahn–Teller coupling constants using the methods of Bacci and find the following:

$$\langle xz|\frac{\partial V}{\partial Q(b_{1g})}|xz\rangle = -\langle yz|\frac{\partial V}{\partial Q(b_{1g})}|yz\rangle = +\frac{\partial e_\pi}{\partial r},$$
$$\langle xz|\frac{\partial V}{\partial Q(b_{2g})}|xz\rangle = -\langle yz|\frac{\partial V}{\partial Q(b_{2g})}|yz\rangle = +2e_\pi, \tag{2}$$

using the vibrational phases as given by Bersuker.[24] These equations predict sizable Jahn–Teller coupling within the ^2E_g state. The ground state b_{2g} bending vibration is 190 cm^{-1}, and the predicted coupling $2e_\pi$ is some 12 times this vibrational energy, so the L_zS_z spin-orbit matrix element within the ^2E_g state would be expected to be completely quenched.

However, when we recalculate the ligand field energy levels with this matrix element set to zero (last column, Table II), we arrive at only a slightly smaller spin-orbit splitting of 250 cm^{-1}. In other words, the net spin-orbit splitting of the ^2E_g state of $CuCl_4^{2-}$ ion does not depend directly on the spin-orbit matrix elements within the ^2E_g state, but rather with the matrix elements which connect this state to the nearby $^2B_{2g}(xy)$ and $^2A_{1g}(z^2)$ states.

Previous studies of the vibrational fine structure on the $^2B_{1g} \rightarrow {}^2E_g$ transition have not detected the spin-orbit splitting into Γ_6, Γ_7 states.[25] The calculated splitting is rather similar to the energy interval of the vibrational progression (271 cm^{-1}) so that the latter could mask this splitting due to the spin-orbit coupling. In addition the b_{2g} bending vibration is also expected to be active in the spectrum which will tend to broaden the structure of this transition. In the MCD spectrum, however, an analysis of the vibrational structure of this transition reveals two Franck–Condon progressions with a positive and a negative MCD sign, the latter 265 cm^{-1} to higher energy. This result is in good agreement with the expected spin-orbit splitting and also matches the expected MCD signs (see below).

E. MCD selection rules

We have previously quantified the axial and transverse MCD for a number of different cases for the tetragonally distorted CuF_6^{4-} ion.[26–28] The present study can be compared to those cases where Cu(II) is doped into a cubic host. This results in Jahn–Teller distorted tetragonally elongated $Cu\ ^{II}L_6$ species being formed with local D_{4h} symmetry, and occurs for the cubic $KZnF_3$ (Ref. 29) and MgO (Ref. 30) hosts, where in the MCD experiment, there is a statistical mixture

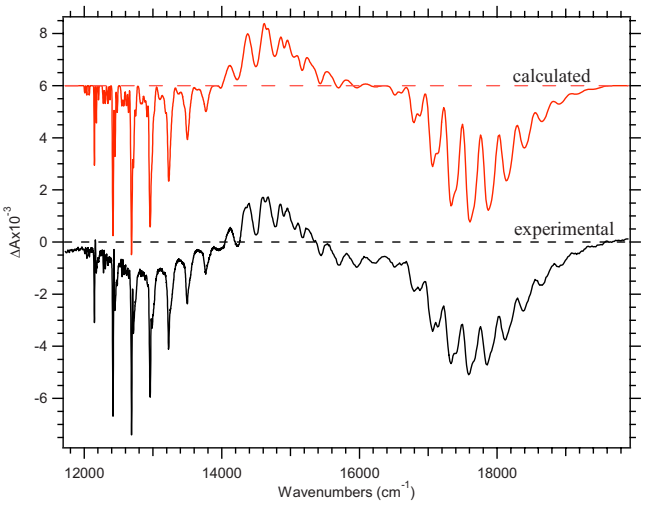

FIG. 4. (Color online) The experimental (bottom) and simulated (top) MCD spectra of the ligand field bands. The parameters used in the simulation are given in Table III.

of 1/3 axial and 2/3 transverse species as encountered here. The lowest energy (observed) ligand field transition is also the $^2B_{1g}(x^2\text{-}y^2) \rightarrow {}^2B_{2g}(xy)$ transition. The predicted and observed sign of the MCD is negative for a magnetic dipole allowed transition.[29] This is in agreement with the negative sign of the MCD observed in this work for the electronic origin of same transition in $CuCl_4^{2-}$.

The $^2B_{1g}(x^2\text{-}y^2) \rightarrow {}^2B_{2g}(xy)$ and $^2B_{1g}(x^2\text{-}y^2) \rightarrow {}^2A_{1g}(z^2)$ transitions both show an overall negative MCD, while that of the $^2B_{1g}(x^2\text{-}y^2) \rightarrow {}^2E_g(xz,yz)$ transition is positive to lower and negative to higher energy. This situation leads to a pseudo-*A* term, typical of transitions to the *E* state in copper(II) compounds with tetragonal symmetry.[31] It is unclear why vibronic origins of the $^2B_{1g}(x^2\text{-}y^2) \rightarrow {}^2B_{2g}(xy)$, $^2A_{1g}(z^2)$ transitions are negative, as the MCD of the lowest LMCT transitions shown in Fig. 2 are predominantly positive. Group theory does not determine the sign, as in the $C_{4h}{}^*$ and $C_{2h}{}^*$ double groups appropriate for the axial and transverse fields, e_u vibrations are active in inducing both left and right circularly polarized transitions. An explicit model which incorporates both the ligand orbitals and vibronic coupling constants for the wavefunctions is required.

F. Variable temperature variable field MCD

It is expected that the absorption intensity of ligand field bands would be temperature dependent due to the vibronic intensity mechanism. However, it proved difficult to follow the intensity changes as the vibrational structure quickly broadened with temperature, so the weak bands became lost in the background.

Figure 5 shows the variable temperature variable field (VTVH) MCD dependence at the wavelengths 805, 568, and 425 nm corresponding to the $^2B_{1g}(x^2\text{-}y^2) \rightarrow {}^2B_{2g}(xy)$, and $^2B_{1g}(x^2\text{-}y^2) \rightarrow {}^2A_{1g}(xy)$ transitions and the lowest energy LMCT band respectively at a temperature of 1.8 K. The curves for other temperatures overlay this data on the $\beta H/2kT$ scale as expected for $S=\frac{1}{2}$ ground state. The three curves have been normalized to unity, revealing subtle differences. For example, the curve for the $^2B_{1g}(x^2\text{-}y^2) \rightarrow {}^2B_{2g}(xy)$ transition (open circles) rises more steeply than the others. The VTVH behavior of $S=1/2$ systems is well known[32,33] and for the present situation with 1/3 axial and 2/3 transverse, the MCD is given by

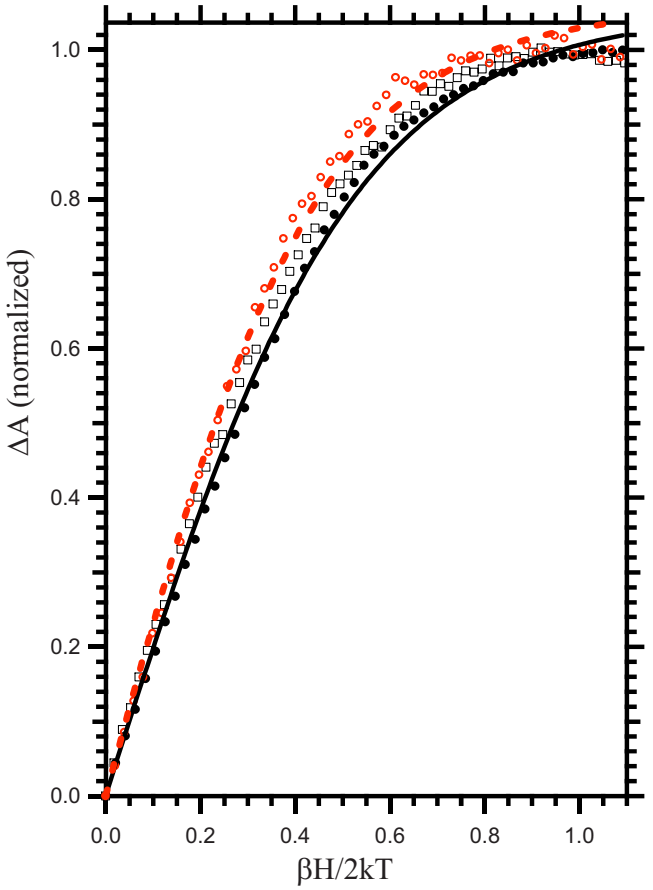

FIG. 5. (Color online) The MCD saturation curves measured at 1.8 K between 0 and 7.0 T at λ=425 nm (filled circles), 586 nm (squares), and 805 nm (open circles) normalized to 1.0. The lines are calculated values using the *g*-values from the EPR (Table I) with the 805 nm data fit to an *xy* polarized transition ($M_\parallel$=1.0; $M_\perp$=0; dashed) and a the 425 nm data to a transition with $M_\parallel$=−0.844 $M_\perp$=0.947 (solid).

$$\Delta A \propto M_\parallel \tanh(g_\parallel \beta H/2kT) + 2M_\perp \tanh(g_\perp \beta H/2kT), \quad (3)$$

where $M_\parallel$ and $M_\perp$ are phenomological parameters that can be fitted to experiment.[32] They can be interpreted as products of the transition moment $M_\parallel = m_x m_y$ and $M_\perp = m_x m_z = m_y m_z$, and so contain information on the polarization of the transitions.

Using the *g*-values from the EPR, the VTVH curves can be reproduced using Eq. (3) with suitable combinations of $M_\parallel$ and $M_\perp$. The data for the $^2B_{1g}(x^2\text{-}y^2) \rightarrow {}^2B_{2g}(xy)$ transition are best fit with $M_\perp=0$, indicating that the transition is *xy* polarized ($m_z=0$). The $^2B_{1g}(x^2\text{-}y^2) \rightarrow {}^2A_{1g}(z^2)$ and LMCT transitions require similar values for $M_\parallel$ and $M_\perp$ indicating that these transitions are allowed in both xy and z polarization. This agrees with the vibronic selection rules given below.

G. Vibrational fine structure

The vibrational fine structure in the spectrum is mainly due to a progression in the totally symmetric stretch of the $CuCl_4^{2-}$ ion. This vibration is at 271, 262, and 272 cm^{-1} in the B_{2g}, E_g, and A_{1g} states, respectively. These values are very similar to those found in other planar $CuCl_4^{2-}$ complexes, being slightly reduced from the ground state value of 275 cm^{-1}. The details of the vibrational fine structure in each transition is due to the different vibronic (false) origins that are allowed for each transition.

The $CuCl_4^{2-}$ complex has the four ungerade vibrations: a_{2u}, b_{2u}, $e_u(s)$, and $e_u(b)$ capable of providing electric dipole intensity via vibronic coupling. The vibronic selection rules are readily evaluated from direct products[17] in the orbital basis to give the following. The $^2B_{1g}(x^2\text{-}y^2) \rightarrow {}^2B_{2g}(xy)$ transition is vibronically allowed in the xy polarization by e_u vibrations and is forbidden in the z polarization. The $^2B_{1g}(x^2\text{-}y^2) \rightarrow {}^2E_g(xz,yz)$ transition is vibronically allowed in the xy polarization by a_{2u}, b_{2u} vibrations, and in the z polarization by e_u vibrations. The $^2B_{1g}(x^2\text{-}y^2) \rightarrow {}^2A_{1g}(z^2)$ transition is vibronically allowed in the xy polarization by e_u and in z by b_{2u} vibrations.

The xy polarized nature of the lowest energy $^2B_{1g}(x^2\text{-}y^2) \rightarrow {}^2B_{2g}(xy)$ transition agrees with the VTVH analysis given above. The relatively high resolution available in this system has allowed us to assign five vibronic origins, the two most intense of which are due to one quantum of the e_u vibrations in the excited state. The additional three weak features we assign to coupling to lattice modes.

H. Franck–Condon progression and excited state geometries

The Franck–Condon intensity patterns can be fitted to a displacement between ground and excited state potential energy surfaces of $D=2.5$, 2.72, and 3.0 (in dimensionless units) for transitions to the B_{2g}, E_g, and A_{1g} excited states (Table III). The slight increase in D with the increasing energy of the transition is evident in the spectra. The Franck–Condon maximum of the $^2B_{1g}(x^2\text{-}y^2) \rightarrow {}^2B_{2g}(xy)$ transition is at $n=2$, while that of the $^2B_{1g}(x^2\text{-}y^2) \rightarrow {}^2A_{1g}(z^2)$ transition is at $n=3$.

The change in the individual Cu–Cl bond lengths (in picometer) is related to the dimensionless displacement D by the expression $\Delta r = \frac{1}{2}D/[1.722\times10^{-3}\sqrt{\mu\bar{\nu}}]$, where μ is the reduced mass (in amu) and $\bar{\nu}$ is the wavenumber of the vibration.[19] This gives the values $\Delta r = +7.4$, +8.2 and +8.8 pm for the change of all four Cu–Cl bond lengths at the equilibrium geometry of the B_{2g}, E_g, and A_{1g} excited states, respectively.

A simple expression for predicting the bond length change in an electronic transition that changes the electronic configuration of the d-orbitals has previously been given.[34] Substituting the values appropriate for the present system, one predicts $\Delta r = +8.9$, +10.5 and +12.5 pm for the respective transitions. Thus the expression lead to a slight overestimation of the experimental values.

IV. CONCLUSIONS

The Cu(II) ion is present in the Cs_2ZrCl_6 lattice as the square planar $CuCl_4^{2-}$ species. A $CuCl_4^{2-}$ ion replaces a $ZrCl_6^{2-}$ center and axial coordination is completely absent. The d-d transitions of the $CuCl_4^{2-}$ ion shows very well resolved vibrational structure. The lowest energy $^2B_{1g}(x^2\text{-}y^2) \rightarrow {}^2B_{2g}(xy)$ transition has a magnetic dipole allowed origin at 12 166 cm^{-1} with a half width of ~10 cm^{-1}.

A Franck–Condon analysis shows an increase in the bond lengths by 7.4 pm accompanying this transition, smaller than previously observed in pure copper compounds with the square planar $CuCl_4^{2-}$ ion. All d-d transitions are shifted to slightly higher energy. These observations suggest that the host lattice relaxes significantly about the $CuCl_4^{2-}$ impurity ion.

For the first time, the splitting of ^2E_g state has been observed. This was possible as the two split components of the MCD spectra have opposite signs. We have also demonstrated that while this state is expected to have a strong Jahn–Teller coupling, the quenching of the spin-orbit coupling within this state does not affect the overall observed splitting. The splitting is principally determined by coupling with other states.

[1] R. G. McDonald, M. J. Riley, and M. A. Hitchman, Inorg. Chem. **27**, 894 (1988).
[2] L. Antolini, A. Benedetti, A. C. Fabretti, and A. Giusti, Inorg. Chem. **27**, 2192 (1988); R. L. Harlow, W. J. Wells, G. W. Watt, and S. H. Simonsen, *ibid.* **13**, 2106 (1974); H. C. Nelson, S. H. Simonsen, and G. W. Watt, J. Chem. Soc., Chem. Commun. 632 (1979); M. J. Riley, D. Neill, P. V. Bernhardt, C. H. L. Kennard, and K. Byriel, Inorg. Chem. **37**, 3635 (1998); M. R. Udupa and B. Krebs, Inorg. Chim. Acta **33**, 241 (1979).
[3] V. M. Masters, M. J. Riley, and M. A. Hitchman, Chem. Phys. Lett. **288**, 743 (1998).
[4] C. Chow, K. Chang, and R. D. Willett, J. Chem. Phys. **59**, 2629 (1973).
[5] M. A. Hitchman and P. J. Cassidy, Inorg. Chem. **18**, 1745 (1979).
[6] M. J. Riley, Inorg. Chim. Acta **268**, 55 (1998).
[7] R. K. Szilagyi, M. Metz, and E. I. Solomon, J. Phys. Chem. A **106**, 2994 (2002).
[8] G. Engel, Z. Kristallogr. **90**, 341 (1935).
[9] J. E. Bray, Phys. Rev. B **18**, 2973 (1978).
[10] S. Maniv, A. Reuveni, and Z. Luz, J. Chem. Phys. **66**, 2285 (1977).
[11] M. J. Riley, E. R. Krausz, and A. Stanco, J. Inorg. Biochem. **96**, 217 (2003).
[12] G. R. Hanson, K. E. Gates, C. Noble, M. Griffin, A. Mitchell, and S. Benson, J. Inorg. Biochem. **98**, 903 (2004).
[13] D. Piehler, W. K. Kot, and N. Edelstein, J. Chem. Phys. **94**, 942 (1991).
[14] R. K. Yoo and T. A. Keiderling, J. Phys. Chem. **94**, 8048 (1990).
[15] T. G. Harrison, H. H. Patterson, and J. J. Godfrey, Inorg. Chem. **15**, 1291 (1976).
[16] S. R. Desjardins, K. W. Penfield, S. L. Cohen, R. L. Musselman, and E. I. Solomon, J. Am. Chem. Soc. **105**, 4590 (1983).
[17] M. A. Hitchman and M. J. Riley, in *Inorganic Electronic Structure and Spectroscopy*, edited by E.I. Solomon and A.B. P. Lever (Wiley, New York, 1999), Vol. 1, p. 213.
[18] S. V. Didziulis, S. L. Cohen, A. A. Gewirth, and E. I. Solomon, J. Am. Chem. Soc. **110**, 250 (1988).
[19] M. J. Riley and M. A. Hitchman, Inorg. Chem. **26**, 3205 (1987).
[20] M. J. Riley, C. Boutchard, E. R. Krausz, and M. A. Hitchman, Chem. Phys. Lett. **254**, 403 (1996).
[21] M. Gerloch and R. F. McMeeking, J. Chem. Soc. Dalton Trans., 2443 (1975).
[22] H. H. Patterson, T. G. Harrison, and R. J. Belair, Inorg. Chem. **15**, 1461 (1976).
[23] R. Englman and A. Yahalom, J. Mol. Struct. **838**, 24 (2007).
[24] I. B. Bersuker, *The Jahn-Teller Effect and Vibronic Interactions in Modern Chemistry* (Plenum, New York, 1984), p. 15.
[25] R. G. McDonald and M. A. Hitchman, Inorg. Chem. **25**, 3273 (1986).

[26] M. J. Riley, L. Dubicki, G. Moran, E. R. Krausz, and I. Yamada, Chem. Phys. **145**, 363 (1990).
[27] D. Reinen, G. Steffen, M. A. Hitchman, H. Stratemeier, L. Dubicki, E. R. Krausz, M. J. Riley, H. E. Mathies, K. Recker, and F. Wallrafen, Chem. Phys. **155**, 117 (1991).
[28] M. J. Riley, L. Dubicki, G. Moran, E. R. Krausz, and I. Yamada, Inorg. Chem. **29**, 1614 (1990).
[29] L. Dubicki, M. J. Riley, and E. R. Krausz, J. Chem. Phys. **101**, 1930 (1994).
[30] A. K. Dick, E. R. Krausz, K. S. Hadler, C. Noble, P. L. W. Tregenna-Piggott, and M. J. Riley, J. Phys. Chem. C **112**, 14555 (2008).
[31] S. J. Smith, C. J. Noble, R. C. Palmer, G. R. Hanson, G. Schenk, L. R. Gahan, and M. J. Riley, JBIC, J. Biol. Inorg. Chem. **13**, 499 (2008).
[32] F. Neese and E. I. Solomon, Inorg. Chem. **38**, 1847 (1999).
[33] P. N. Schatz, R. L. Mowry, and E. R. Krausz, Mol. Phys. **35**, 1537 (1978); A. J. Thomson, M. R. Cheesman, and S. J. George, Methods Enzymol. **226**, 199 (1993).
[34] M. A. Hitchman, Inorg. Chem. **21**, 821 (1982).